

POLARIZATION FEATURES OF X-RAY RADIATION EMITTED NEAR BLACK HOLES

PAUL A. CONNORS,¹ TSVI PIRAN,² AND RICHARD F. STARK¹

Received 1979 May 7; accepted 1979 July 9

ABSTRACT

We compare the X-ray polarization features of geometrically thick clouds surrounding a black hole and the standard accretion disk model. The calculations include a fully general-relativistic treatment of the radiation transfer problem. In both cases general-relativistic corrections can lead to large rotations in the plane of X-ray polarization and to changes in the degree of polarization. Such differences are potentially observable and can be used to distinguish between the two models. The polarization features can indicate whether a black hole is present in a compact X-ray source.

Subject headings: black holes — polarization — relativity — X-rays: sources

I. INTRODUCTION

Two major problems persist in the study of compact X-ray sources: verification of a given astrophysical model, and the demonstration of the existence of a black hole in any particular source.

In a recent review paper Eardley *et al.* (1978) conclude that there is as yet no definite evidence for the existence of a black hole in Cygnus X-1. They describe a variety of models which have been suggested for the structure of the accretion disk in this system. The models have been compared with observations mainly according to the resulting spectra. Almost all such work has excluded general-relativistic effects and has used the Newtonian approximation when constructing disk models and spectra. Novikov and Thorne (1973) and Page and Thorne (1974) have derived the general-relativistic corrections to the disk structure equations. These are of order unity for a Schwarzschild black hole but can become important and affect the spectrum for rapidly rotating black holes.

An additional source of information about the disk structure is the X-ray polarization features. This was first pointed out by Rees (1975) and by Lightman and Shapiro (1975), who used the Newtonian results of Chandrasekhar (1960) and Angel (1969) to determine the polarization from accretion disks. Stark and Connors (1977) and Connors and Stark (1977) have pointed out that, unlike the spectrum, the polarization features are strongly affected by general-relativistic effects.

In this work we describe an attempt to explore in detail the polarization features of radiation from two general-relativistic accretion configurations: a standard accretion disk (Shakura and Sunyaev 1973; Pringle and Rees 1972; Novikov and Thorne 1973), and a geometrically thick cloud accreting onto a black hole (Thorne and Price 1975; Shapiro, Lightman, and Eardley 1976).

For disk calculations we determine the polarization transfer function for propagation of X-rays to an observer at infinity, and use it to derive the observed polarization properties. A numerical Monte Carlo method is used to solve the general-relativistic radiative transfer problem for the thick-cloud case.

As would be expected, the polarization features are different for such different emitting configurations. In both configurations, general-relativistic corrections are important, and it is completely misleading to predict polarization features of an accretion disk by using a Newtonian approximation.

In particular, the Newtonian results, by symmetry, allow only two possible directions for the plane of polarization. The fast Keplerian rotation near the black hole breaks this symmetry, and general-relativistic effects (which can be larger than the special-relativistic aberration [Stark and Connors 1977]) allow polarization angles in any direction. Detection of continuous rotation of the polarization plane as a function of energy or time in a particular compact X-ray source can serve, therefore, as additional support for the existence of a black hole in that system.

For the case of disk accretion, one may expect a variation of the polarization angle and degree of polarization with energy (more energetic photons coming from nearer the black hole suffer larger general-relativistic rotations). For isothermal clouds, such a variation with energy is not expected for the part of the spectrum emitted by the cloud. Softer X-rays, coming from the outer disk, will have a different polarization angle. Lightman and Shapiro (1975) used the Newtonian approximation to predict a 90° jump in the angle of polarization. Because of the general-relativistic corrections, the jump will no longer be 90°.

¹ Department of Astrophysics, Oxford University.

² Center for Relativity, The University of Texas, Austin.

Novick *et al.* (1977) reported a marginally significant detection of 3% linear polarization at an energy of 2.6 keV from Cyg X-1. This single measurement is insufficient. More observations are needed in order to learn, from the polarization features, about the nature of the compact object and of the accretion process in this system.

The general theory of polarization propagation in the Kerr metric, polarization induction by Compton scatterings, and numerical methods are discussed in § II. In § III we describe the Newtonian calculations of polarization from disks and clouds. The general-relativistic results for disks and clouds are described in §§ IV and V. Finally, the astrophysical implications are discussed in § VI.

II. GENERAL THEORY AND NUMERICAL METHODS

a) Polarization Induced by Electron Scattering

The polarization of a beam of radiation can be described by the normalized Stokes parameters (Chandrasekhar 1960):

$$X_s = Q/I, \quad Y_s = U/I, \quad (1)$$

where I is the intensity and Q , U are the Stokes parameters determining the linear polarization. As the polarization is induced by Compton scattering, there is no circular polarization for initially unpolarized radiation.

X_s and Y_s range between ± 1 , and they are defined relative to a chosen 2-axis e_1, e_2 such that e_1, e_2 are spacelike and orthogonal to the wave vector k . The degree of polarization, δ , and the angle of the plane of polarization, ψ , are given by

$$\delta = (X_s^2 + Y_s^2)^{1/2}; \quad \psi = \frac{1}{2} \tan^{-1} (Y_s/X_s). \quad (2)$$

The direction of polarization of a beam of radiation is described by a unit four-vector, f , which is orthogonal to the wave vector k . The normalized cross section for the scattering of a polarized beam from a direction k to k' (where, if k is regarded as defining a z -axis and e_1, e_2 the (x, y) -axis, then Θ, Φ are the usual angular coordinates of the k' direction) is given by (Berestetskii, Lifshitz, and Pitaevskii 1971)

$$\frac{d\sigma}{d\Omega}(\Theta, \Phi) = \frac{C}{Z^2} \left[Z + \frac{1}{Z} - \sin^2 \Theta - \sin^2 \Theta (X_s \cos 2\Phi + Y_s \sin 2\Phi) \right],$$

where

$$C = \left\{ \frac{2\pi}{\eta} \left[(1 - 2/\eta - 2/\eta^2) \log(1 + 2\eta) + \frac{1}{2} + \frac{4}{\eta} - \frac{1}{2(1 + 2\eta)^2} \right] \right\}^{-1},$$

$$Z = 1 + \eta(1 - \cos \Theta),$$

$$\eta = E_{e1}/m_e c^2, \quad (3)$$

and where E_{e1} is the energy of the incoming photon in the electron's rest frame, and m_e is the electron mass. For an unpolarized beam, this is the Klein-Nishina cross section.

The Stokes parameters of the scattered beam, X_s' and Y_s' , measured relative to a new 2-axis e_1', e_2' with e_1' in the scattering plane defined by k, k' , and e_2' perpendicular to it, are given by

$$X_s' = \frac{1}{N} [\sin^2 \Theta - (1 + \cos^2 \Theta)(X_s \cos 2\Phi + Y_s \sin 2\Phi)],$$

$$Y_s' = \frac{1}{N} 2 \cos \Theta (X_s \sin 2\Phi - Y_s \cos 2\Phi),$$

$$N = Z + 1/Z - \sin^2 \Theta - \sin^2 \Theta (X_s \cos 2\Phi + Y_s \sin 2\Phi). \quad (4)$$

b) Parallel Transport and Polarization Rotation

The polarization vector, f , is parallelly transported along the photons null geodesic, i.e.:

$$\nabla_k f = 0 \quad \text{and} \quad k \cdot f = 0 \quad (5)$$

where ∇_k is the covariant derivative along the null ray. The degree of polarization is a scalar invariant.

The spacetime around a black hole is described by the Kerr metric (Kerr 1963); we shall use the Boyer-Lindquist coordinates (t, r, θ, φ) (Boyer and Lindquist 1967; Misner, Thorne, and Wheeler [MTW] 1973). One should note that, for large radii, the Boyer-Lindquist radial coordinate r approaches the Newtonian distance from the origin and hence can be used to describe Newtonian radial distances in this regime. We use geometrical units ($c = G = 1$) and measure distances in gravitational radii of the black hole, whose mass is M .

The transport of the polarization vector is determined by the properties of geodesic motion. Every geodesic in the Kerr metric is described by three constants of motion: E/μ and L/μ (where μ is the particle's rest mass and E and L are the energy and angular momentum as measured by an observer at infinity) and Q/μ^2 (Carter's constant) (Carter 1968; De Felice 1968; Wilkins 1972; MTW 1973).

Walker and Penrose (1970) have discovered a fourth complex constant, κ_{pw} , which is conserved along null geodesics in the Kerr metric. This constant, which is related to Carter's constant, is used to describe the parallel transport of the polarization vector f (Connors and Stark 1977):

$$\begin{aligned} \kappa_{pw} = \kappa_2 - i\kappa_1 = & \{(k^0 f^1 - k^1 f^0) + a \sin^2 \theta (k^1 f^3 - k^3 f^1) \\ & - i[(r^2 + a^2)(k^3 f^2 - f^3 k^2) - a(k^0 f^2 - k^2 f^0)] \sin \theta\} (r - ia \cos \theta). \end{aligned} \quad (6)$$

A given null geodesic (with a given polarization vector) through a point (t, r, θ, φ) is characterized by L/E , Q/E , and κ_{pw}/E . The wave vector, k , is determined from the geodesic equations (for example, MTW 1973) while equation (6) together with $k \cdot f = 0$ and $f \cdot f = 1$ is solved for f . For an observer at infinity the Stoke's parameters can be expressed directly in terms of the constants of motion:

$$\begin{aligned} X_\infty &= \delta(S\kappa_1 - T\kappa_2)/(S^2 + T^2), \\ Y_\infty &= \delta(-S\kappa_2 - T\kappa_1)/(S^2 + T^2), \end{aligned} \quad (7)$$

where $S = (L/\sin \theta_0 - a \sin \theta_0)$, $T = \text{sgn}(\kappa^\theta)_\infty (Q - L^2 \cot \theta_0 + a^2 \cos^2 \theta_0)^{1/2}$, and X_∞ , Y_∞ are defined relative to the fixed 2-axis e_θ , e_φ at infinity for an observer with polar angle θ_0 .

The polarization properties are Lorentz-transformed in the following way: the degree of polarization, δ , is a Lorentz invariant. The unit four-vector f is only defined to within a multiple of k . We can therefore always choose $f = (0, \cos \psi e_1 + \sin \psi e_2)$ with $X = \delta \cos 2\psi$, $Y = \delta \sin 2\psi$. Let f' and k' be the Lorentz-transformed f and k . The quantity f' can be rewritten in the form

$$f' = \left(0, f'^i - \frac{f'^0 k'^i}{k'^0}\right) = (0, \cos \psi' e_1' + \sin \psi' e_2') \quad (i = 1, 2, 3),$$

where now $X' = \delta \cos 2\psi'$, $Y' = \delta \sin 2\psi'$.

c) The Spectral and Polarization Transfer Functions

Cunningham (1975) defines a transfer function, F , which relates the local spectral properties at the disk's surface to those seen by a particular observer at infinity. We denote by a subscript e quantities at the rest frame of the emission radius r_e , and by a subscript 0 quantities observer at infinity at polar angle θ_0 .

For a given geometrically thin disk model the locally emitted intensity I_e is a function of E_e , r_e and n_e , the angle between the normal to the disk and the direction in which the ray leaves the disk. The observed flux is (Cunningham 1975):

$$I_0(E_0, \theta_0) = \iint 2\pi I_e(E_0/g, n_e, r_e) F(g^*, r_e, \theta_0) g^2 (g^* - g^{*2})^{-1/2} dg^* d(\pi r_e^2), \quad (8)$$

where $g = E_0/E_e$, and $g^* = (g - g_{\min})/(g_{\max} - g_{\min})$ and where g_{\max} (or g_{\min}) is the maximum (or minimum) redshift for rays reaching θ_0 from r_e .

All possible orbits linking the emission point to the chosen observing angle θ_0 are included as g^* varies from 0 to 1 to 0 (i.e., F is double-valued in g^*).

We define the polarization transfer function, h , as $F e^{2i\psi}$, where ψ is the direction of polarization measured at infinity (relative to e_θ , e_φ) for a ray whose initial plane of polarization lies in the plane of the disk. If the initial plane of polarization differs from this by, say, an angle β , then ψ is simply increased by β .

The net Stokes parameters, \bar{Q} , \bar{U} , can then be expressed as

$$\bar{Q}(E_0) + i\bar{U}(E_0) = \iint 2\pi I_e \delta_e h g^2 (g^* - g^{*2})^{-1/2} dg^* d(\pi r_e^2). \quad (9)$$

The observed degree of polarization and the polarization angle $\bar{\delta}(E_0)$, $\bar{\psi}(E_0)$ are:

$$\bar{\delta}(E_0) = (\bar{Q}^2(E_0) + \bar{U}^2(E_0))^{1/2} / \bar{I}(E_0), \quad (10a)$$

$$\bar{\psi}(E_0) = \frac{1}{2} \tan^{-1} [\bar{U}(E_0)/\bar{Q}(E_0)]. \quad (10b)$$

d) The Geometrically Thin Disk

Following the transfer functions approach described earlier, the calculation of the observed features of the radiation seen from a geometrically thin disk is divided into two stages: determination of the local properties of

the emitted radiation, and evaluation of the propagation effects from the source to the observer. This approach has been used by Cunningham (1976) and by Payne and Eardley (1977) to calculate spectral features of accretion disks. A photon scattered within an optically thick but geometrically thin disk travels only a small geometrical distance both between scatterings and after the last scattering. The general-relativistic effects during the radiative transfer process are therefore very small and can be neglected. Along with this approximation we use the general-relativistic disk equations, derived by Novikov and Thorne (1973) (see also Page and Thorne, 1974), to evaluate the local emitted spectra I_e , and the Newtonian results of Horak (1954) and Chandrasekhar (1960) (see § III) to prescribe the local polarization properties (δ_e, ψ_e) at the disk's surface. The transfer functions are used to calculate the observed features at infinity.

e) *Geometrically Thick Clouds and Numerical Methods*

As in the thin disk case, the initial polarization features are determined by the local properties on which general-relativistic propagation effects are superposed. However, the local properties can no longer be given by the Newtonian approximation, and for geometrically thick clouds it is necessary to include general-relativistic effects during the radiative transfer within the clouds. We assume that the initial radiation source is not polarized and that the radiation is polarized subsequently by Compton scattering within the cloud. In order to solve this general-relativistic radiation transfer problem, we use a numerical Monte Carlo method. A numerical code, previously developed to calculate radiation transfer in the Kerr metric (Piran and Shaham 1977a), was modified to include polarization and used to study this problem.

The physical input data for each calculation include the density and temperature profiles within the cloud, the average electron motion as a function of position, the initial energy distribution of the photons (relative to the electron rest frame), and the emissivity function.

A starting point for the photon is randomly chosen within the cloud according to the emissivity function. The photon has a random initial direction of motion relative to the bulk matter motion at that point. This determines the photon's constants of motion E, L, Q . The initial photon is unpolarized, and its polarization parameters X_s, Y_s vanish. An optical depth τ is then chosen at random according to the probability function:

$$P(\tau > \tau') = e^{-\tau'}. \quad (11)$$

The equation of motion of the photon is integrated along its null geodesic together with the optical depth that the photon traverses. When the optical depth equals τ , the photon is scattered. The motion of the scattering electron is determined according to the average motion of the cloud at the point of scattering together with a random thermal motion. The scattering angles (Θ, Φ) are chosen at random according to equation (3). These parameters then determine the photon's constants of motion after the scattering (Piran and Shaham 1977b). The new polarization parameters X_s', Y_s' are given by equation (4). After transforming to the Boyer-Lindquist coordinates from the electron's rest frame, the Penrose-Walker constants κ_1 and κ_2 are evaluated.

This process is repeated until the photon escapes from the cloud or falls into the black hole. The escaping photons are classified according to their energy interval and their polar angle, θ_0 , at infinity.

In order to account for time delay effects, a time-dilation factor g_s is calculated for each photon. This quantity g_s allows for the fact that, while the time dilation is proportional to the special- and general-relativistic redshifts, energy changes due to electron recoil in the scatterings do not contribute to the time dilation. The quantity g_s is calculated from:

$$g_s = g / \prod_{i=1}^N (\mathcal{E}_i / \bar{\mathcal{E}}_i), \quad (12)$$

where $\mathcal{E}_i, \bar{\mathcal{E}}_i$ are the photon energies in the electron's rest frame just before and just after scattering, and N is the number of scatterings the photon undergoes before escaping. Note that g_s includes a special-relativistic correction, and for relativistic electrons $T_e \gtrsim 10^9$ K it is important even in flat spacetime calculations. Addition of g_s to Comptonization Monte Carlo calculation (Pozdnyabov, Sokol', and Sunyaev 1976) may drastically change the high-energy shape of the resulting spectrum.

For each energy and angular bin the following sums are computed:

$$\begin{aligned} N(E, \theta_0) &= \text{number of "unweighted" photons in the } E, \theta_0 \text{ bin;} \\ I(E, \theta_0) &= \sum g_s; \\ X_s(E, \theta_0) &= \left(\sum X_s g_s \right) / I(E, \theta_0); \\ Y_s(E, \theta_0) &= \left(\sum Y_s g_s \right) / I(E, \theta_0). \end{aligned} \quad (13)$$

The energy spectrum is given by $I(E, \theta_0)$. The degree of polarization, δ , and the polarization angle, ψ , are found from:

$$\begin{aligned}\delta &= (X_s^2(E, \theta_0) + Y_s^2(E, \theta_0))^{1/2}, \\ \psi &= \frac{1}{2} \tan^{-1} [Y_s(E, \theta_0)/X_s(E, \theta_0)].\end{aligned}\quad (14)$$

The number of energy and angle intervals is varied so that for a given configuration there will be enough photons in each bin to give reasonable statistics. A measure of the standard deviation in such a Monte Carlo calculation is:

$$\Delta(N_{\mathbf{E}}, \theta_0) \sim [N(E, \theta_0)]^{1/2}. \quad (15)$$

This yields the following approximate absolute errors for N , δ , ψ :

$$\begin{aligned}\Delta(N_{\mathbf{E}}, \theta_0) &\sim [N(E, \theta_0)]^{1/2}, \\ \Delta(\delta) &\sim [N(E, \theta_0)]^{-1/2}, \\ \Delta(\psi) &\sim \frac{|X_s| + |Y_s|}{(X_s^2 + Y_s^2)} \frac{1}{[N(E, \theta_0)]^{1/2}}.\end{aligned}\quad (16)$$

For cold clouds, and photon energies much less than $m_e c^2$, we can formulate the Monte Carlo results in terms of integrated polarization “transfer” functions which are independent of the initial photon energy. In such a case and for a fixed initial energy, the observed photon number, $NE(g)$, depends only on the redshift g . $NE(g)$ becomes the integrated (over the cloud) photon number transfer function. As in the previous section, the integrated polarization “transfer” function H is obtained from the observed plane of polarization $\psi(g)$ by:

$$H(g) = NE(g)e^{2i\psi(g)}. \quad (17)$$

We also define $\delta(g)$, the observed degree of polarization. For any particular choice of initial photon number spectrum, $N_e(E_e)$, the observed number Stokes parameters (I , Q , and U divided by the energy), \bar{N} , \bar{N}_Q , \bar{N}_U , can be reconstructed by a convolution of N_e and NE , h , δ over the redshift g .

The variation of $\bar{\psi}$, $\bar{\delta}$ with observed energy at infinity for this choice of initial spectrum are found, as before, from equation (10). Note that these “transfer” functions include the total effects of scattering and propagation within the source and propagation from the source to the observer.

III. NEWTONIAN CALCULATIONS

We consider the polarization properties for two basic geometrical configurations of cold homogeneous electron scattering gas: a plane slab and an ellipsoidal cloud. The matter is cold in the sense that the electron temperature, even though high enough for ionization and for electron scattering to dominate, is much lower than $m_e c^2$. The plane of linear polarization for these configurations is limited to one of two directions only: in the plane of the observer and the symmetry axis (the observer plane), or perpendicular to this. This is due to the mirror symmetry about the equatorial and observer planes in these Newtonian configurations. It is important to note that the superposition of two such perpendicularly polarized beams of radiation will still give a polarization only in one of these planes.

Chandrasekhar (1960), Horak (1954), and Sandford and Pauls (1973) have discussed uniformly emitting slabs of varying optical depths, and Angel (1969) has discussed uniformly emitting ellipsoidal configurations. In general the degree of polarization from these configurations is less than 10%. For both these configurations, when the optical depth is large ($\tau \gg 1$), the plane of polarization is perpendicular to the observer plane; for low optical depths, the plane of polarization is at 90° to this. In both cases the degree of polarization decreases as an observer moves from the equatorial plane toward the pole, vanishing for a polar observer. For intermediate optical depths there may be a zero in the degree of polarization and a subsequent discontinuous jump of 90° in the angle of polarization as the observer angle θ_0 is varied.

We have used our numerical code to reproduce, as a check, the analytic results of Horak for a uniformly emitting slab of optical depth $\tau = 0.2$, and the Monte Carlo results of Angel for an ellipsoid with an axis ratio of 1:3 and optical depth 2 along the semimajor axis. (See the 200 M result of Fig. 11.)

In these calculations, photons are chosen initially distributed homogeneously and isotropically throughout the cloud. We have studied another possibility in which the initial photons are injected radially inward from an axisymmetric exterior source in the equatorial plane, into the ellipsoidal cloud discussed above. This configuration, which may correspond to an outer accretion disk surrounding an inner accreting cloud around a black hole (Thorne and Price 1975; Shapiro, Lightman, and Eardley 1976), has the advantage that the resulting degree of polarization is around 20% (compared to 5% for the homogeneously emitting cloud), and the results are correspondingly more accurate statistically.

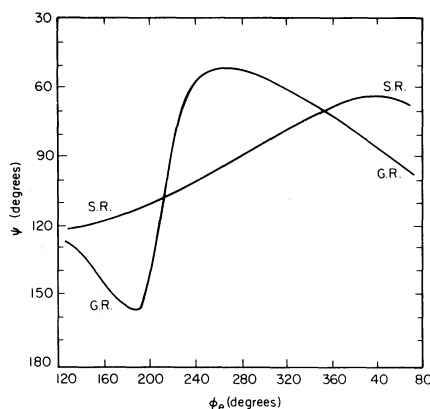


FIG. 1.—Special and general relativistic polarization angle for rays emitted at the equatorial plane of a Kerr black hole ($a/M = 0.998$) $r_e = 6.25M$, $\theta_0 = 41^\circ.4$. The initial polarization direction in the equatorial plane.

The polarization angle is 180° (plane of polarization in the observer plane) for observers in the equatorial plane. The degree of polarization decreases as θ_0 decreases, but the angle remains 180° . At a certain observer angle there is a 90° jump in the polarization angle, accompanied by a vanishing degree of polarization (see $200 M$ cloud in Fig. 12). This behavior manifests that there are only two polarization directions in the Newtonian configurations.

IV. THE GENERAL RELATIVISTIC DISK

a) Polarization Rotations from Infinitesimal Disk Elements

We first describe the polarization rotations as a function of the position of emission for points orbiting in the equatorial plane around a black hole. These rotations determine the contributions seen at infinity from infinitesimal emitting elements of the disk's surface. The polarization angle ψ is measured by the observer at infinity using the fixed axis e_θ , e_ϕ . Figures 1 and 2 compare the special- and general-relativistic polarization angles ψ_{SR} , ψ_{GR} for emission sources orbiting a Kerr black hole. The angle ψ_{SR} can be obtained from

$$\cot \psi_{SR} = \cos \theta_0 \cos \phi_e / (\sin \phi_e + v^{-1} \sin \theta_0), \quad (18)$$

where ϕ_e is the azimuthal angle and v is the orbital velocity. The corresponding Newtonian result is $\psi = 90^\circ$ (independent of ϕ_e).

The difference between the special- and general-relativistic results can be understood by:

1. The change in the local angle of emission, n_e , resulting from the gravitational bending of the orbit. This leads to a difference in the contributions to ψ_{SR} , ψ_{GR} from the aberration due to the rotation of the emitting source.

2. The general-relativistic Fermi-Walker rotation along the orbit from emission to observer.

The contributions from general- and special-relativistic effects can be of equal importance for quite large radii (especially for observers with small polar angles).

For a given equatorial ring ψ is a double-valued function of g^* , the normalized redshift parameter (see Fig. 3). The first g^* range (0, 1) corresponds to orbits coming predominantly from behind the black hole; the second range (1, 0), to those coming from the front. As the ring's radius decreases, the $g^* = 1$ rays are emitted from farther behind the black hole and are swept around in azimuth to reach the observer. Due to the factor $g^2(g^{*2} - g^*)^{-1/2}$ in equations (8) and (9), the contribution of those maximum blueshifted rays ($g^* \sim 1$) dominates the emission

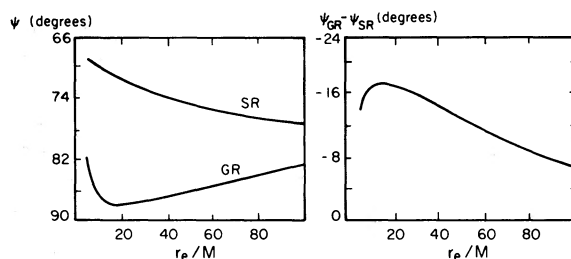


FIG. 2.—Special and general relativistic polarization angles for sources orbiting a Schwarzschild black hole. The azimuthal angle is fixed, $\phi_e = 65^\circ$, $\theta_0 = 5^\circ$. The initial polarization direction is in the equatorial plane.

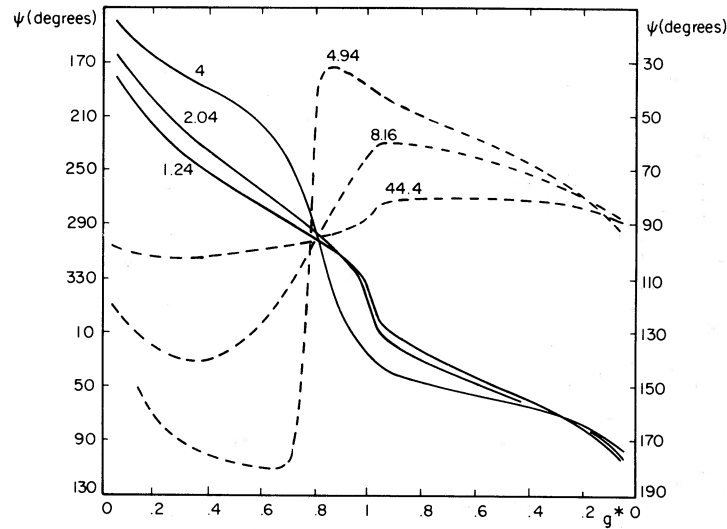


FIG. 3.—General relativistic polarization angle as a function of g^* , for $r < r_{\text{crit}}$ (solid line, left ordinate) and for $r > r_{\text{crit}}$ (dashed line, right ordinate): $\theta_0 = 41.4$ and $a/M = 0.998$.

from the whole ring. This is more distinct when the difference between g_{max} and g_{min} is large, i.e., for a small emission radius and for an observer near the equatorial plane.

The variation of ψ with g^* is divided into two types of behavior—for emission radii above and below r_{crit} , which is approximately determined by the first vanishing of the denominator in equation (18). The general-relativistic corrections shift r_{crit} slightly from the special relativistic value given by equation (18).

b) Orbiting “Hot Spots”

An isotropically emitting polarized source of radiation (“hot spot”) orbiting a black hole at constant radius will be observed to have, in addition to time-varying spectrum and intensity, a time-varying polarization angle. Figure 4 shows such time variation of the polarization plane (light travel time delay across the orbit is included). The angle remains roughly constant, within a few degrees, and then wobbles by $\sim 20^\circ$ in a small fraction of the period. For smaller r_e the fraction of the period occupied by the wobble gets smaller (compare Pineault 1977). (In Fig. 4 only the direct, most intense, light paths have been considered, i.e., those that do not pass through the equatorial plane after emission.) Note that for hot spots orbiting at smaller radii, multiple imaging effects (Cunningham and Bardeen 1973) must be included.

c) Integration over the Standard Disk Model

A standard accretion disk is characterized by the mass M of the black hole, \dot{M} the accretion rate, and α viscosity parameter (see, for example, Shakura and Sunyaev 1973). As an example we use $M = 9 M_\odot$, $\dot{M} = 7 \times 10^{17} \text{ g s}^{-1}$, and $\alpha = 0.1$. Variation of these parameters over the range of astrophysically relevant values does not cause any qualitative changes in the results. For these parameters the disk is optically thick ($\tau_{\text{es}} > 1$) throughout.

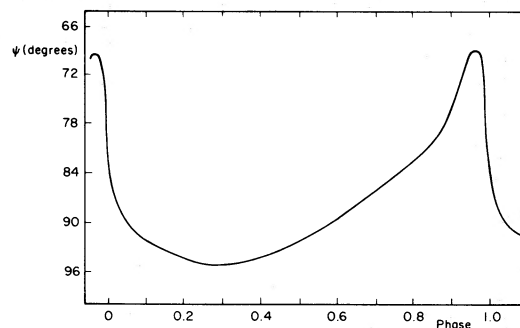


FIG. 4.—The observed plane of polarization from a hot spot orbiting a Kerr black hole ($a/M = 0.998$) in the equatorial plane. $r_e = 11.1M$, the orbit's period is $239M$, $\theta_0 = 75.5$. Initial polarization direction is in the equatorial plane. The hot spot is directly behind the black hole when the phase is zero.

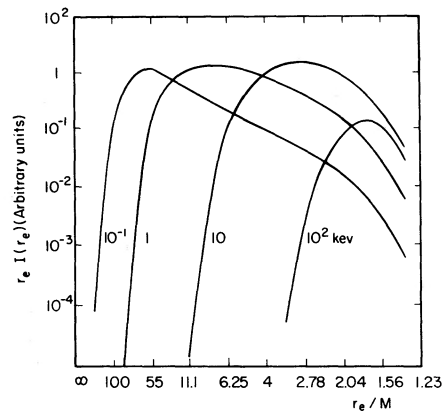


FIG. 5.—The observed flux from an emitting ring which is a part of a standard disk: $a/M = 0.998$, the disk parameters are $M = 9 M_{\odot}$, $\dot{M} = 10^{17} \text{ g s}^{-1}$, and $\alpha = 0.1$, $\theta_0 = 75^\circ 5'$.

Before studying the integrated results, we discuss the polarization of radiation coming from particular rings of this disk.

Figure 5 shows the intensity observed at infinity of the radiation emitted by rings with equal widths which are parts of a standard disk. As expected, the higher the energy, the smaller the radius from which it is predominantly coming (e.g., for $E_0 = 10 \text{ keV}$, the radiation is predominately coming from $r_e \sim 3M$).

The polarization properties from such rings are shown in Figures 6a and 6b. The plane of polarization from these emitting rings is almost independent of energy. Notice that for the near equatorial observer the properties of the smaller rings essentially reflect those of the maximum blueshifted radiation ($g^* \sim 1$). This results from the factor of $g^2(g^{*2} - g^*)^{-1/2}$ in equation (9) which is very large for small r_e values. This picking out of the maximum blueshifted rays is less important for smaller θ_0 . The falloff of polarization at larger radii is due to the dominating influence of the free-free opacity over the electron opacity, while variations at smaller radii are due to the depolarizing effect of adding together radiations with differently rotated polarization planes, and to orbit-bending and subsequent changes in n_e .

The single-ring results are integrated to give the net observed properties as a function of observing energy. The final integrated results for the disk parameters indicated are shown in Figures 7 and 8a, b, c, d.

The intensity spectra for rapidly rotating black holes are significantly changed from those for Schwarzschild ones and display a high-energy tail. The polarization rotations at high energies are also different.

These rotations are clearly large enough to be observed. The differences from Newtonian values increase as θ_0 decreases. The sense of the rotation is such that an observer above the disk ($\theta_0 < 90^\circ$) sees a clockwise rotation with increasing energy, and those below it see a counterclockwise rotation.

Below $\sim 0.1 \text{ keV}$ there is no polarization (Fig. 8b, d) because of free-free opacity. At higher energies the polarization increases. In the absence of general-relativistic effects it would increase to the constant value given by Chandrasekhar's result ($\sim 0.9\%$ for $\theta_0 = 41^\circ 4'$, 4.7% for $75^\circ 5'$). However, above $\sim 1 \text{ keV}$ the depolarizing effect of adding together polarization planes with different amounts of gravitational rotation causes it to decrease. At this energy (1 keV), photons are coming mainly from a radius $\sim 10M$, and it is here that the plane of polarization

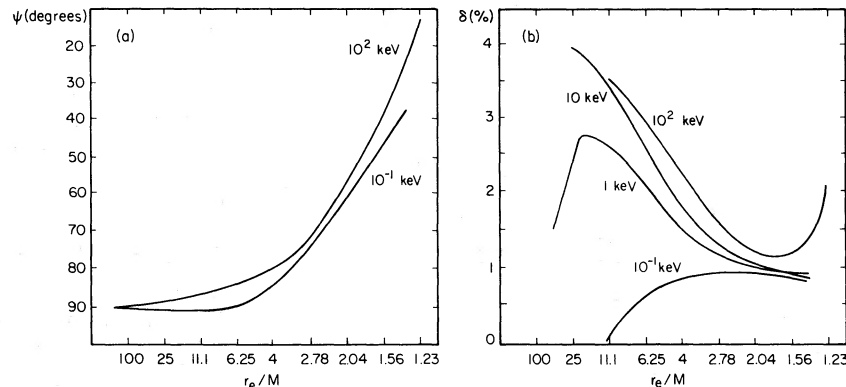


FIG. 6.—Polarization features from rings (parameters as for Fig. 5). (a) Polarization plane, ψ , for two extremes (0.1 and 100 keV) of the observed energy range. (b) Degree of polarization for various observed energies.

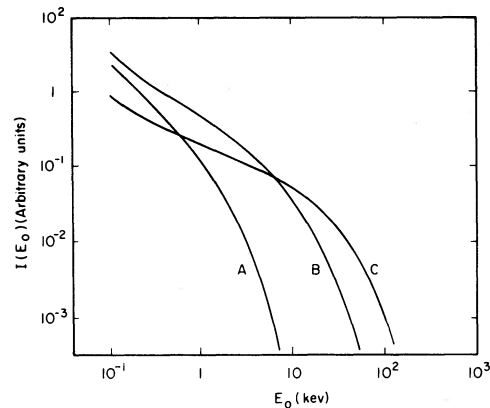


FIG. 7.—The observed flux spectrum for the standard disk model. Disk parameters are as in the text: *A*, Schwarzschild black hole, $\theta_0 = 41^\circ.4$. *B*, Kerr black hole ($a/M = 0.998$), $\theta_0 = 41^\circ.4$. *C*, Kerr black hole ($a/M = 0.998$), $\theta_0 = 75^\circ.5$.

starts to rotate appreciably. Beyond a minimum at ~ 25 keV the polarization increases again (slowly for $a/m = 0$, more rapidly for maximal Kerr) because of strong field effects.

V. GENERAL RELATIVISTIC CLOUDS

We study oblate ellipsoidal mass configurations (clouds) centered on a Kerr black hole. The clouds are homogeneous, isothermal, optically thin, and cold (as discussed earlier). This study is motivated by the geometrically thick accretion cloud (Thorne and Price 1975). However, the clouds do not correspond directly to any specific model. Rather, we examine a series of clouds whose geometry is similar to Angel's (1969) ellipsoidal configuration (an oblate ellipsoid with a 1:3 ratio of axes) with a black hole added in the center.

The size of the cloud serves as a natural general-relativistic parameter. For large clouds, the Newtonian region dominates and the results correspond to the Newtonian limit (Angel 1969). Thus, we investigate the general-relativistic effects by varying the size of the clouds, freezing as much as possible the same physical conditions. Specifically, the optical depth along the cloud is kept constant, although the density is not.

Generally, the polarization features for an equatorial observer resemble the Newtonian results (though there may be changes in the degree of polarization). The relativistic effects become prominent as the observer moves toward the poles. In particular, the relativistic clouds display a minimum in the degree of polarization for an intermediate observer angle. For rotating clouds this minimum is associated with rotation of the polarization plane. The relativistic minimum appears nearer to the equatorial plane, and the associated dip ranges over a larger span of observer angles for more relativistic configurations.

All the configurations that we study contain homogeneous, isothermal, cold, and optically thin clouds ($\tau = 1$ to 2). Unlike the polarization features of relativistic accretion disks, the polarization features of these clouds do not depend on the photon's energy (for $E \ll m_e c^2$). This behavior distinguishes the homogeneous cloud configuration from geometrically thin accretion disks and can serve as an observational test between these models.

Other physical effects are studied by changing various parameters, one at a time. The following configurations are considered:

- | | |
|---|---|
| i) Size of cloud (r is the length of the semimajor axis) | $5 M < r < 200 M$ (the minimum radius is larger for the smaller a/m black holes); |
| ii) Initial photon distribution | Uniform and isotropic or equatorial axisymmetric external source; |
| iii) a/m of the black hole | 0 (Schwarzschild), 0.9, 0.95, 0.998 |
| iv) Gas motion | Generalized circular motion, or radial infall. |

We also consider effects of varying the shape of the clouds and their optical depth. Finally we examine possible effects of a surrounding sphere of gas with optical depth $0 < \tau < 1.5$.

The optical depth along the semimajor axis is kept constant in most of the configurations studied, i.e., $\tau = 2$.

The inner boundary of the clouds is defined by r_{mb} . For this, we extend (Piran 1976; Piran and Shaham 1977a) the definition of r_{mb} (Bardeen *et al.* 1972) from the equatorial plane to a general circular orbit. In general $r_{\text{mb}}(\text{nonequatorial}) > r_{\text{mb}}(\text{equatorial})$. This structure corresponds to fast infall of matter from the innermost region of the cloud into the hole.

The gas motion can break the symmetry of the cloud. Rotation, for example, breaks the mirror symmetry about the equatorial plane. This allows the polarization plane to vary continuously in direction, instead of being confined to two directions as in the Newtonian cases. In our rotating clouds the average motion at a point (r, θ) is such that a particle remains with the same r value and is at its maximal (minimal) θ point. This condition on the θ motion

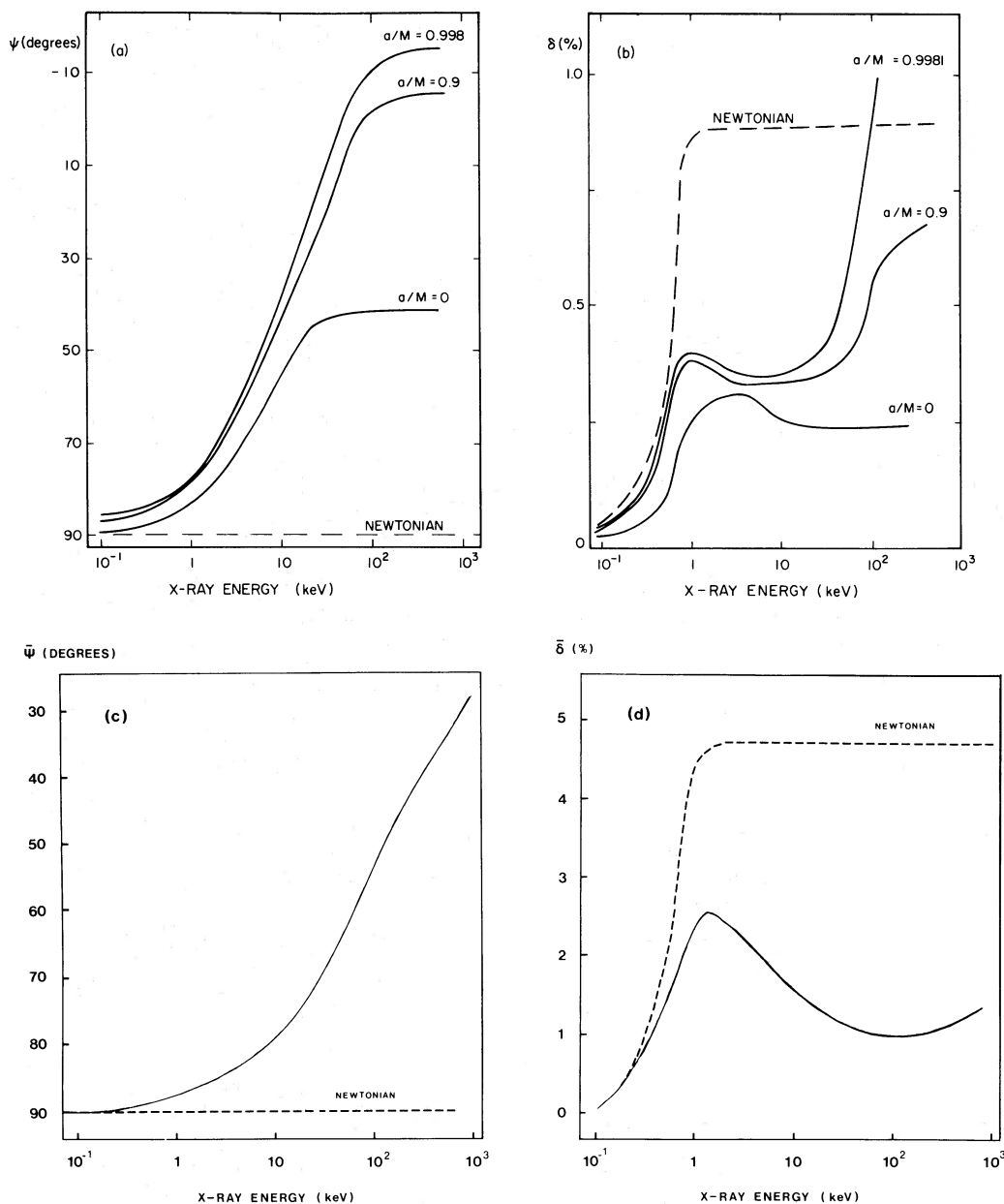


FIG. 8.—Polarization features from a standard disk model (parameters as in the text) for various values of a/M . (a) Polarization angle, ψ , $\theta_0 = 41^\circ.4$. (b) Degree of polarization, δ , $\theta_0 = 41^\circ.4$. (c) Polarization angle, ψ , $\theta_0 = 75^\circ.5$, $a/m = 0.998$. (d) Degree of polarization, δ , $\theta_0 = 75^\circ.5$, $a/m = 0.998$.

is necessary in the Kerr metric in order to define the orbits (Wilkins 1972). This motion reduces to circular motion in the equatorial plane and to general circular motion in the Newtonian regime.

The radial infall cases that we have looked at correspond to the infall of the gas from rest and with zero angular momentum at infinity ($E = \mu$, $L = Q = 0$). In these cases, for a Schwarzschild black hole, the symmetry is preserved and the polarization plane is confined to two directions.

An initial power law spectrum, $N_e \propto E^{-\alpha}$, remains unchanged under convolution with the integrated transfer function $NE(g)$. This means that for a homogeneous, isothermal cloud with an initial power law spectrum the polarization properties are independent of the observed photon energy (for $E \ll m_e c^2$). Moreover, our results show that the polarization properties do not vary greatly for $-3 < \alpha < 0$, which is the relevant astrophysical regime. In the following discussion we present, therefore, results for an initial flat, $\alpha = 0$, spectrum. These results can be easily compared with the Newtonian results in which $g = 1$ throughout.

The results of the Monte Carlo calculations are presented in Figures 9–15. In all these figures polarization angles differing by 180° are equivalent. The averaging over finite angular size, introduced by the Monte Carlo method, results in some smoothing of discontinuous jumps and in nonvanishing polarization near the pole. The actual polarization drops to zero only for $\theta_0 \leq 10^\circ$ for many of the cases studied.

a) Rotating Clouds

i) Uniform and Isotropic Initial Photon Distribution

The photon number transfer function $NE(g)$ and the degree and plane of polarization $\delta(g)$, $\psi(g)$ are shown in Figures 9 and 10 for two clouds with semimajor axis of $200 M$ and $10 M$. A few basic features emerge from this: For the $200 M$ cloud the range of g is very small and the polarization angle is around 180° . For the smaller cloud the intensity is characterized by a systematic redshift of the whole spectrum as the observer angle moves toward the pole. The degree of polarization is always smallest for the redshift with maximum intensity, where it is around a few percent (i.e. of the same order as the Newtonian result). The degree of polarization is consistently higher for the blueshifted part of the spectrum.

The Newtonian optically thin cloud (Angel 1969) has an angle of polarization of 180° (in the observer plane). This is also the case for an equatorial observer viewing a relativistic cloud. However, as θ_0 decreases, a 180° rotation of the polarization angle as a function of g occurs. This rotation is centered on the intensity peak with the angle of polarization around 90° at the g with maximum intensity. The observer angle for which this transition occurs depends on the size of the cloud, and it moves toward the equator as the cloud shrinks and becomes more relativistic.

The convoluted properties for an initial flat, $\alpha = 0$, spectrum are shown in Figure 11. As θ_0 decreases, the degree of polarization at first decreases as in the Newtonian case, but unlike this case it reaches a minimum, then increases and reaches a maximum for $\theta_0 \sim 10^\circ$ before vanishing at the pole. This is accompanied by a smooth rotation of the polarization angle. The observer angle range over which the rotation takes place moves toward the equator and the width of the range widens for the more relativistic configurations. While the polarization angle for equatorial observers is the same as the Newtonian one (in the observer plane), the rotated angle for high θ_0 is $\sim 120^\circ$. This behavior of the convoluted properties can be explained by the dominance of the g values with highest intensity, for slowly varying initial spectra (see Fig. 11).

ii) External Equatorial Source of Radially Infalling Photons

The addition of another preferred direction to the configuration increases the asymmetry, and therefore the degree of polarization increases. In a Newtonian configuration the degree of polarization vanishes and there is a 90° jump in the polarization angle for an observer angle $\theta_0 \sim 45^\circ$. The jump becomes smaller, $\sim 60^\circ$, and it moves toward the equator (up to 70°), as the clouds become more relativistic (see Fig. 12).

One should note the similarity, for radii $\leq 25 M$, between the behavior of the polarization angle in this case and its behavior in the previous homogeneous emission clouds. This may suggest that general-relativistic propagation effects (combined with the similar geometry and electron motion in these two cases) determine this behavior. (Note also the intensity beaming into the equatorial plane, as was found before, for the more relativistic clouds).

b) Infalling Cloud

A radially infalling, uniformly emitting cloud around a Schwarzschild black hole preserves the mirror symmetry about the observer plane. The polarization angle is therefore still limited to two possible directions. The main difference between the Newtonian and general-relativistic results in this case is in the variation of the degree of polarization with the observer angle (see Fig. 13). Unlike the Newtonian cloud (see $200 M$ results of Fig. 13), the degree of polarization from relativistic clouds vanishes (accompanied by a 90° jump in the polarization angle) for a particular observer angle. Again this angle moves toward the equator for smaller (more relativistic) clouds. The

TABLE 1
FRACTION OF PHOTONS CAPTURED BY A KERR BLACK HOLE ($a/m = 0.998$),
FOR THE THREE ELLIPSOIDAL CLOUDS THAT WE HAVE CONSIDERED

Radius of Cloud	Rotating, Uniform Emission	Rotating, External Equatorial Source	Infalling, Uniform Emission
$5 M$	0.207	0.118	0.938
$10 M$	0.091	0.058	0.648
$20 M$	0.042	0.033	0.314
$50 M$	0.014	0.013	0.075
$200 M$	0.003	0.002	0.001

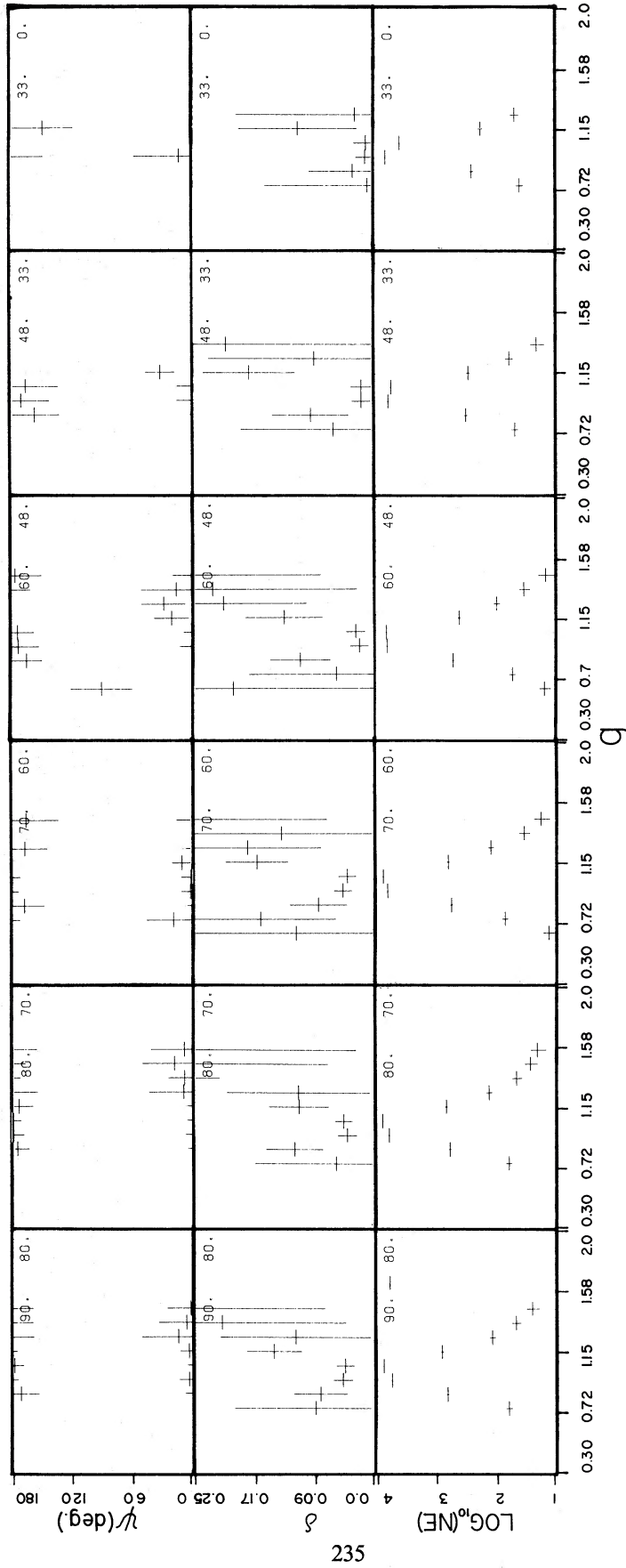


FIG. 9.—Generalized transfer functions for the photon number, $NE(g)$, the degree of polarization, $\delta(g)$, and the polarization angle $\psi(g)$, for six θ_0 ranges, from a uniformly emitting, rotating ellipsoidal cloud. The semimajor axis is $200M$, and the optical depth along it is 2. The axis ratios is 1:3.

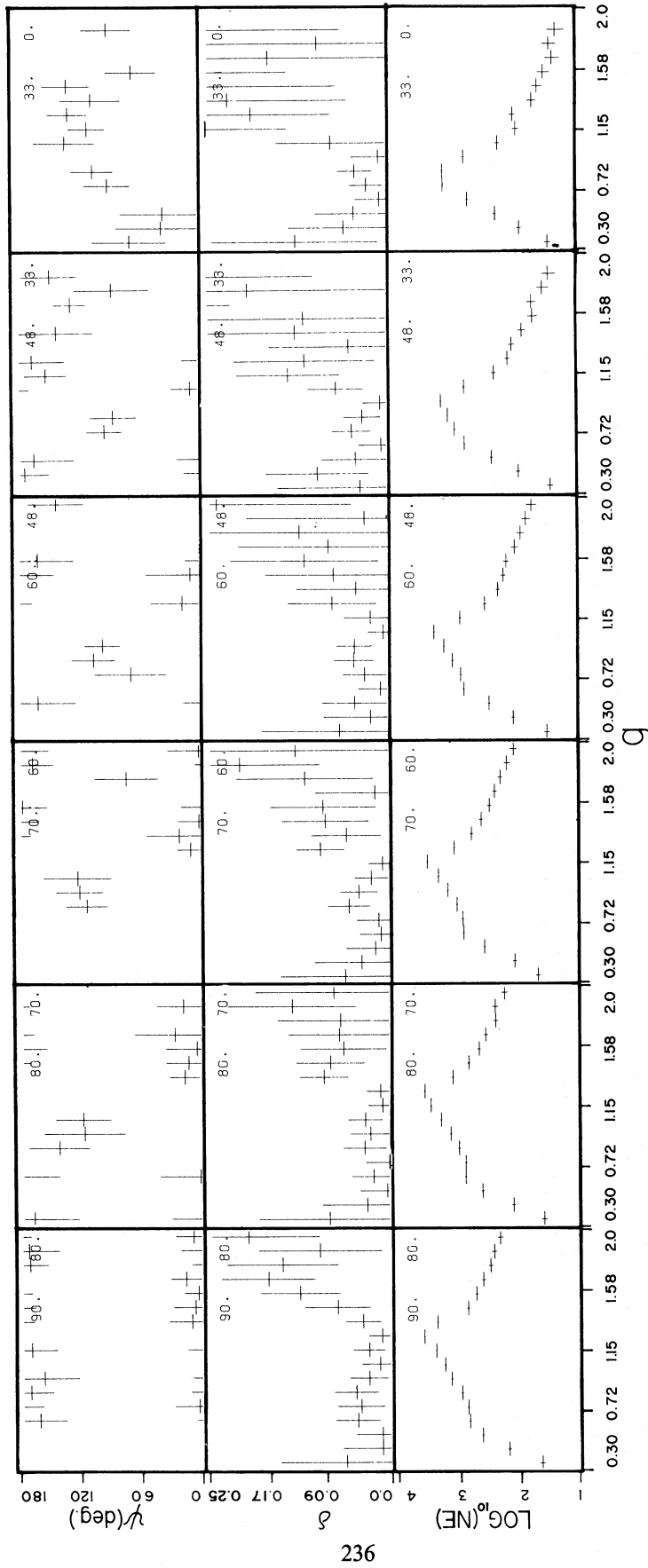


FIG. 10.—Polarization features from a uniformly emitting, rotating cloud for semimajor axis of 10M (details as in Fig. 9)

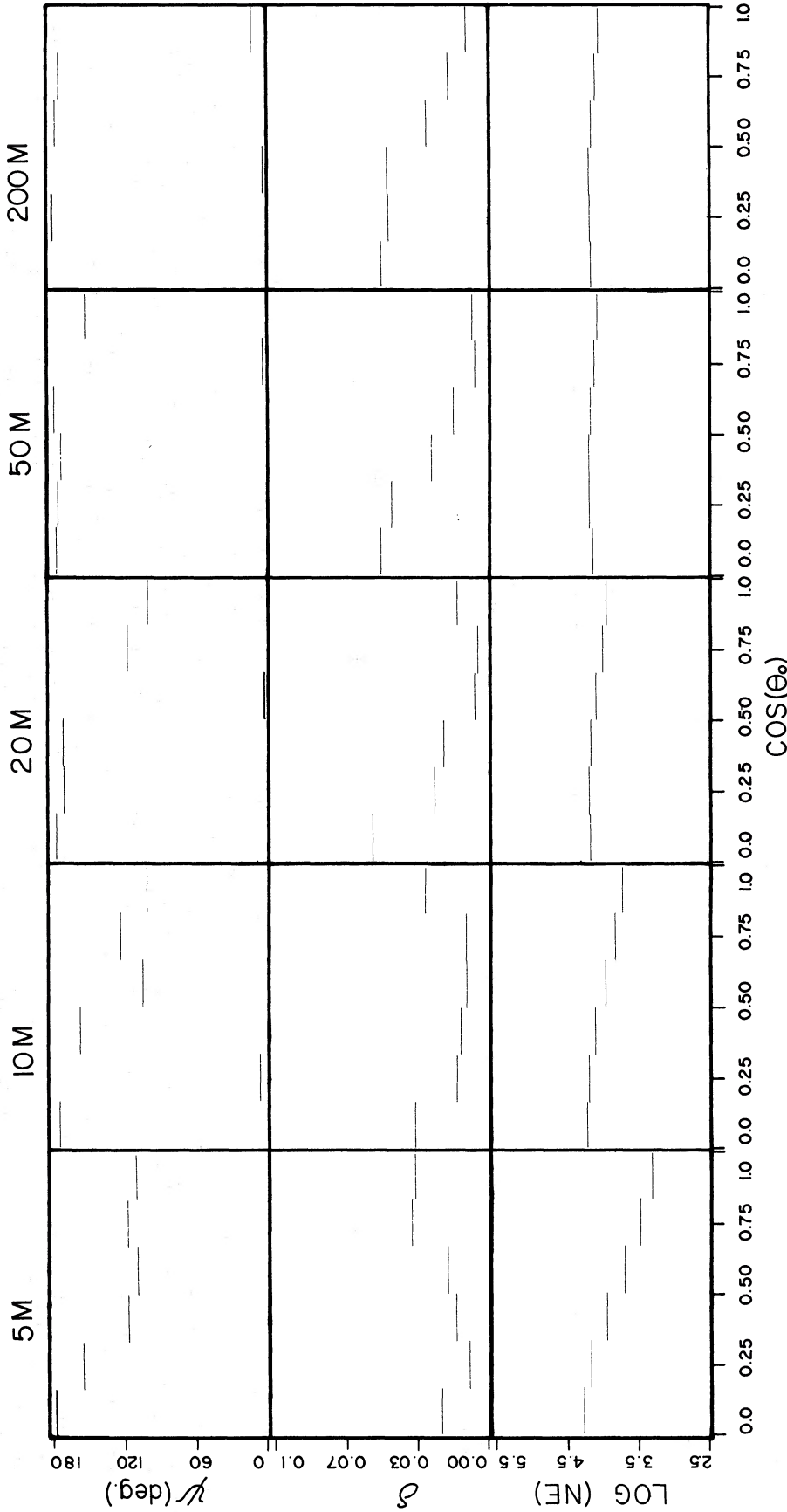


FIG. 11.—Intensity and polarization features from uniformly emitting, rotating clouds of various sizes. The initial photon number spectrum is flat ($N_e \sim E^0$), and the observed polarization features are independent of the observed energy. Cloud details are as for Fig. 9.

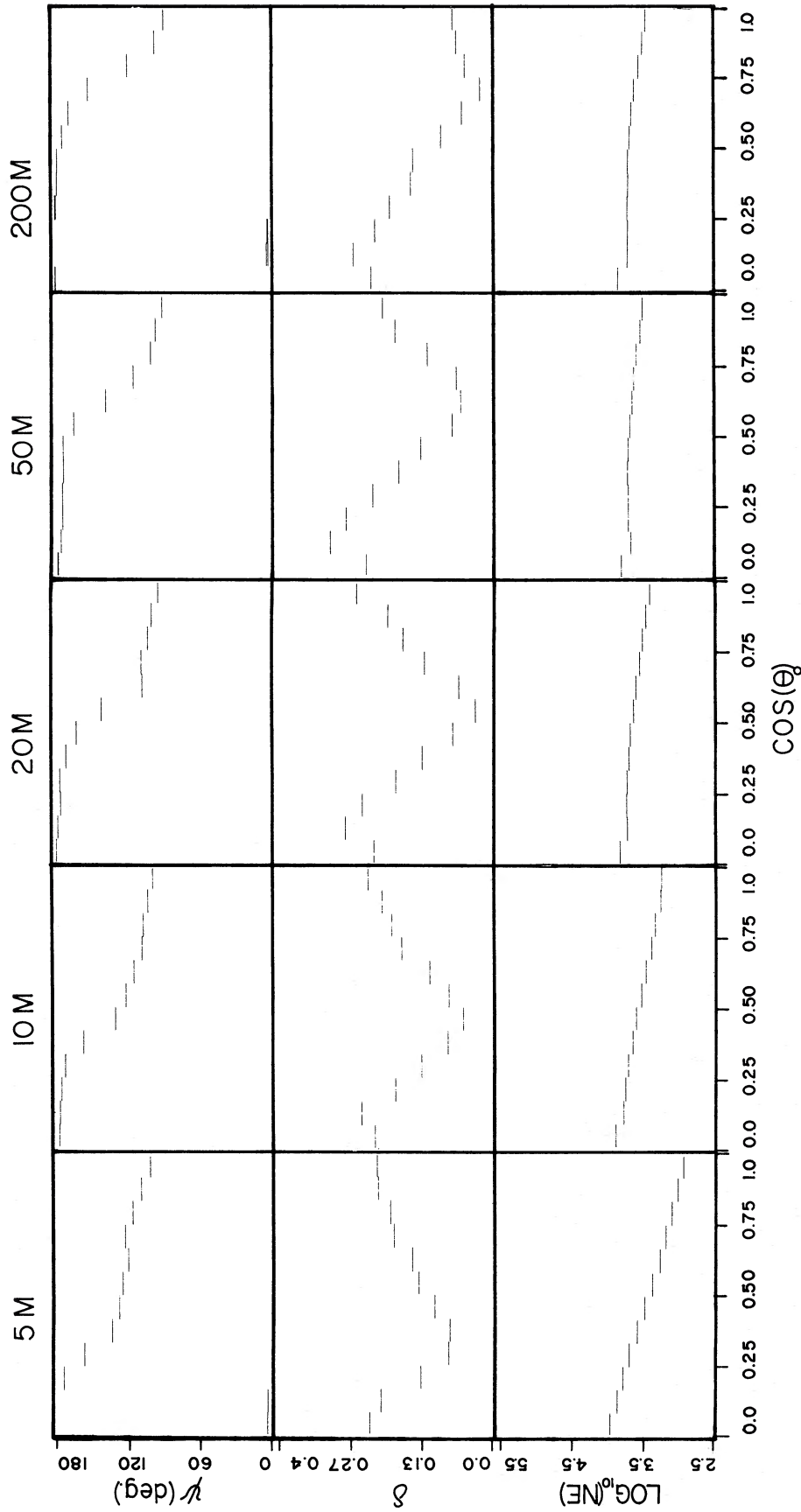


FIG. 12.—Intensity and polarization features from rotating clouds, of various sizes, with an external equatorial photon source (details as in Fig. 11)

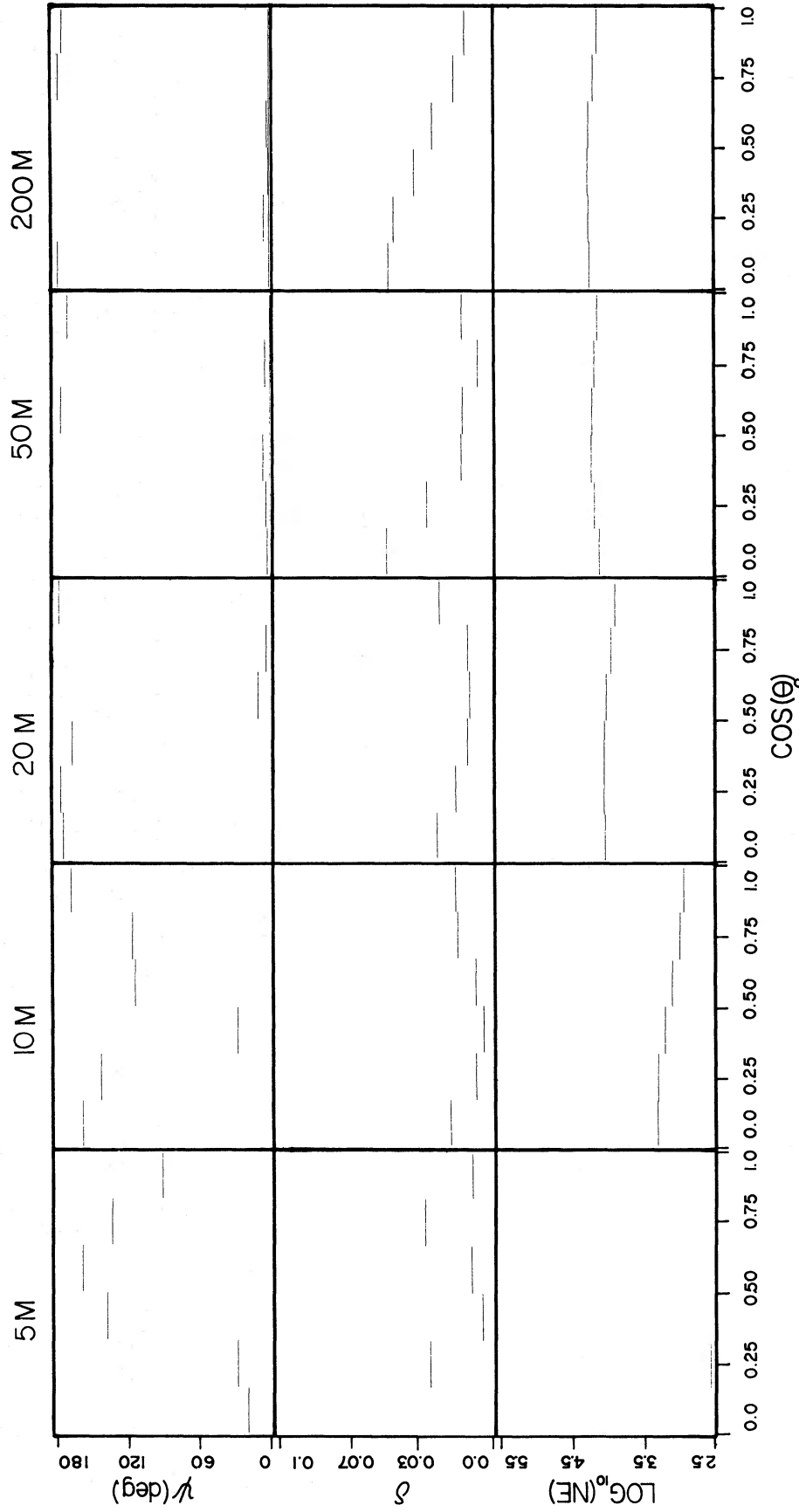


FIG. 13.—Intensity and polarization features from radially infalling, uniformly emitting ellipsoidal clouds of various sizes (details as in Fig. 11)

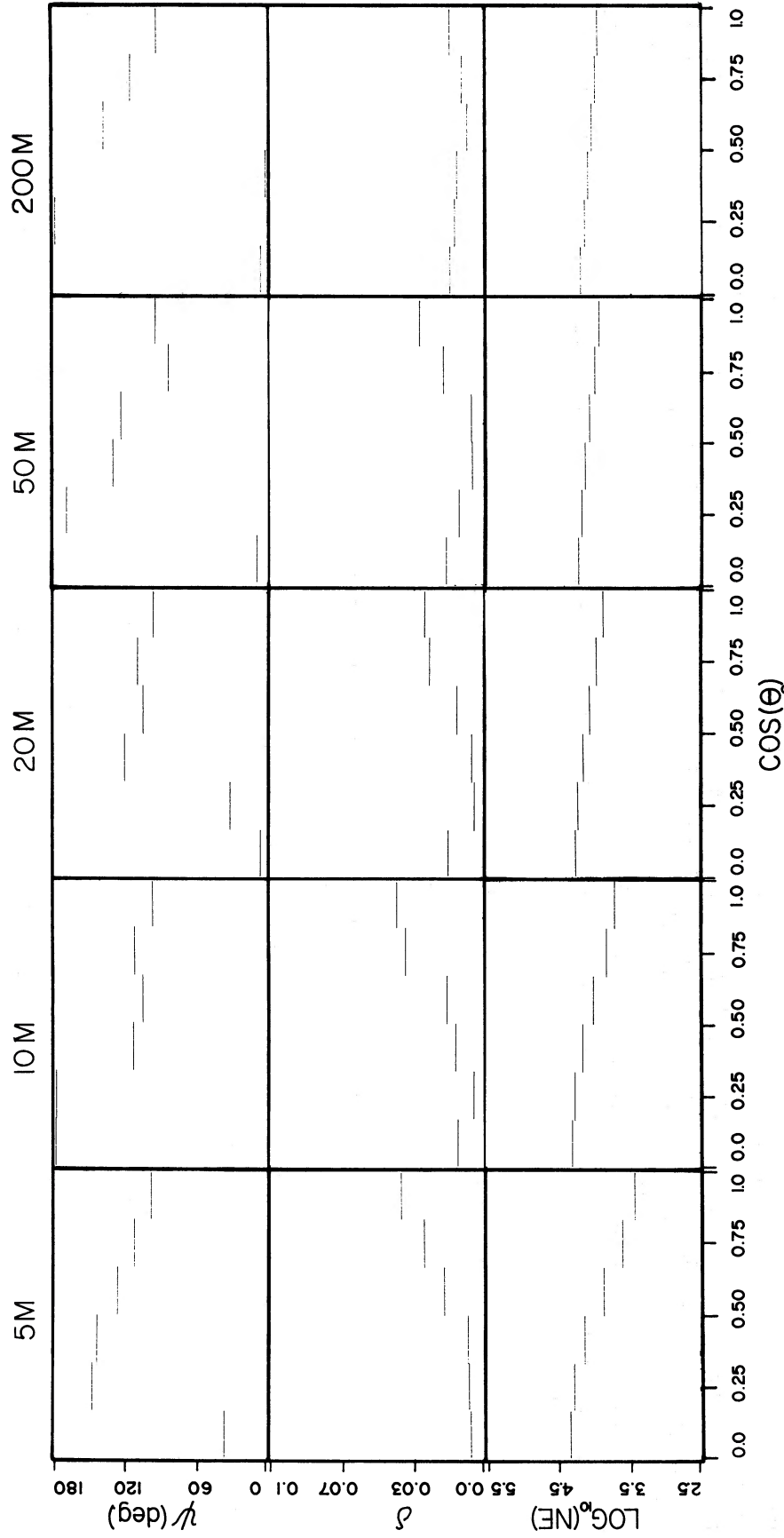


FIG. 14.—Spherical uniformly emitting and rotating clouds of varying radii. Photon number, degree, and plane of polarization against $\cos \theta_0$ for an initial $\alpha = 0$ emission number spectrum are shown ($a/m = 0.998$). The optical depth of the sphere is 1.

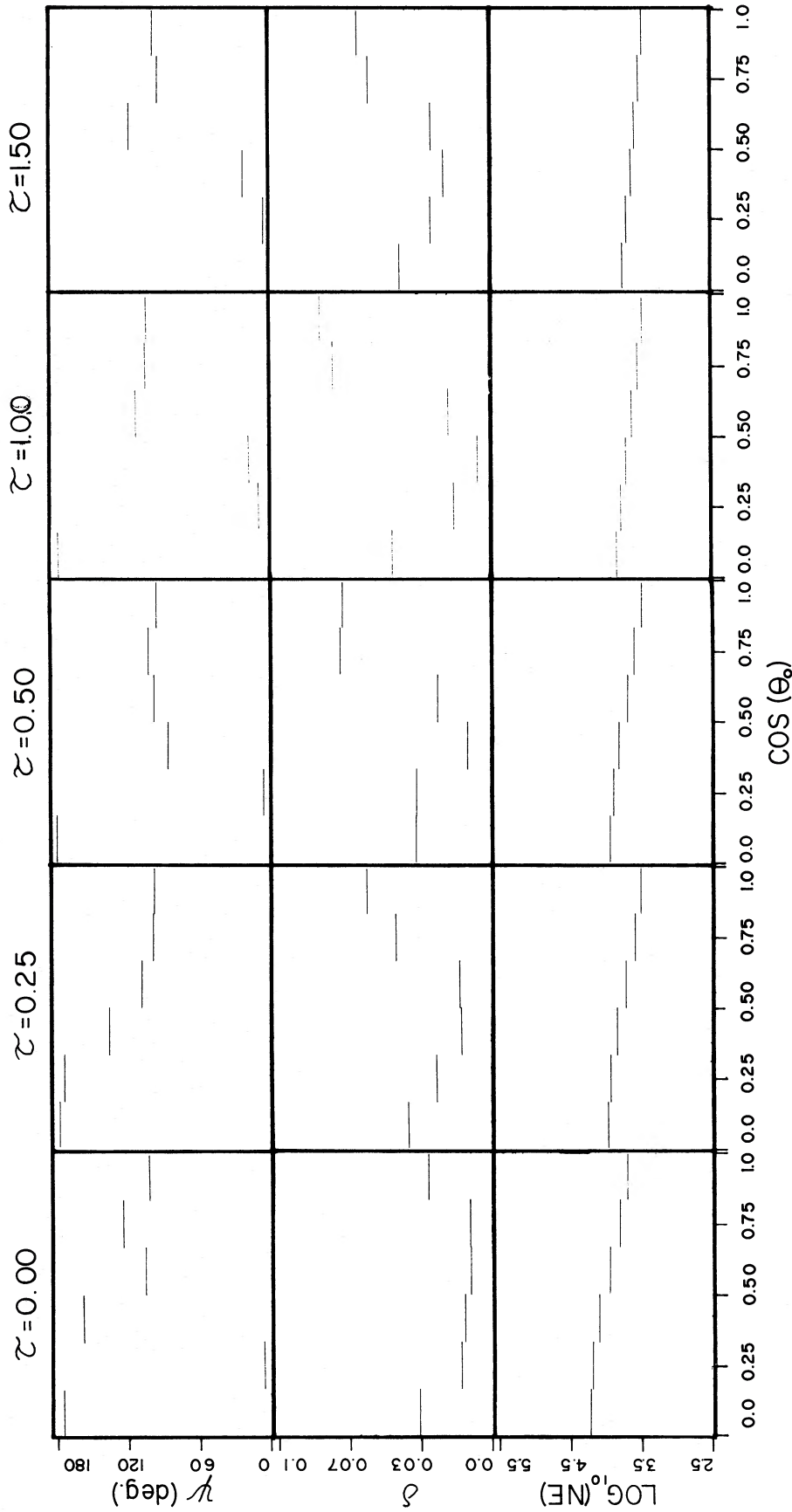


Fig. 15.—Effects of scattering spheres of size $500M$ with various optical depths, τ , surrounding a $10M$ uniformly emitting rotating ellipsoidal cloud. Compare to Fig. 11 for “bare” cloud results.

degree of polarization for small clouds is somewhat less than for the Newtonian cloud. These polarization features do not change strongly when a/m is varied (note that for a Kerr black hole the mirror symmetry about the observer plane is broken).

Intensity beaming into the equatorial plane still occurs for the smaller clouds, although it is reduced compared to the rotating configurations. As expected (Shapiro 1973), many of the photons are captured by the black hole (see Table 1). For example, in a $5 M$ radially infalling cloud around a canonical Kerr black hole, $\sim 94\%$ of the photons are captured by the black hole. The large capture rate for clouds $\lesssim 50 M$ severely limits the statistical accuracy attainable for the smaller sized clouds.

c) Spherical Rotating Cloud

In the very large cloud limit we expect the polarization from very large spherical clouds to vanish (by symmetry). A $200 M$ spherical, rotating cloud gives $\sim 1\%$ polarization (this is due to the small rotational effects still present). Again the smaller and more relativistic spheres show the familiar polarization minimum tending towards the equatorial region and the associated polarization rotation (Fig. 14). There is also a distinctive rise in the polarization for decreasing polar observer angles, for these clouds, reaching a maximum $\sim 3\%$.

d) Angular Momentum (a/m) of the Black Hole

In both cases of uniform emission and equatorial external injection, the resulting polarization features weakly vary with a/m . For clouds of the same radius there are slightly more blueshifted photons for the higher a/m black holes. For large a/m , r_{mb} (the inner boundary of the cloud) approaches the event horizon; and it is possible, therefore, to have smaller clouds in which the general-relativistic effects are more prominent. Effects which depend on a/m vary, usually, as $(a/r)^2$, and, although for a disk the radiation from the innermost region dominates the high-energy regime, in the cloud configuration the contribution of this region is small.

e) Screening by a Surrounding Sphere of Gas

The effects of a large ($r = 500 M$) surrounding gas sphere on the polarization from uniformly emitting rotating $10 M$ cloud are shown in Figure 15. The surrounding sphere does not emit, and its only effect is to scatter the radiation emerging from the inner cloud. The general behavior of the polarization is preserved for the smaller optical depths (i.e., the minimum in the degree of polarization, and the general rotation of the polarization plane). For the larger optical depths, the rotation occurs sharply (over a smaller θ_0 range), and is in conformance with the 90° Newtonian jump.

VI. ASTROPHYSICAL IMPLICATIONS

The importance of polarization as an additional source of information on the accretion processes in X-ray sources was realized by Rees (1975). In this work we have shown that polarization measurements can give information on the strong gravitational fields at the source. The polarization is determined by local processes in the source and by general-relativistic effects within the source and during the propagation to the observer. In general it is difficult to distinguish between the local and general-relativistic contributions. However, a detection of a non- 90° rotation in the angle of polarization (either due to temporal variations or due to observing at different energies) is a good indicator of a strong-field general-relativistic effect.

For a standard disk model the polarization angle shows large variation with energy—corresponding to emission of different energy photons from different regions of the disk. This unique polarization feature, if observed, can indicate both the existence of a black hole in a system and that the accretion is in the form of a standard accretion disk all the way through to the inner region. (Note that the spectrum of a relativistic disk, calculated from Novikov and Thorne 1973 formulae, for an $a/m = 0.9981$ black hole fits the observed spectra much better than a Newtonian disk spectrum [Shakura and Sunyaev 1973]). As in the Newtonian case, the degree of polarization increases as the observer approaches the equatorial plane (compare Figs. 8*b* and 8*d*). The degree of polarization, predicted by the general-relativistic disk model, is however substantially smaller than the Newtonian prediction. This low degree of polarization may limit our ability to observe any polarization from such source unless we are very close to the equatorial plane. In particular, the observation of 3% linear polarization at 2.6 keV from Cyg X-1 (Novik *et al.* 1977), if confirmed, limits the observer angle to Cyg X-1 to $\theta_0 \geq 80^\circ$. Note that this is in agreement with Cunningham's (1975) conclusions which were based on the spectrum of Cyg X-1.

One should proceed with care when applying the results of cold clouds to realistic astrophysical models for which the temperature may be very high (e.g., the central cloud in the two-temperature model, where the electron temperature is around 10^9 K and the photons are inverse Comptonized). However, this approximation has been used in all the Newtonian calculations which have been done so far. Calculations of polarization effects from Newtonian and general-relativistic Comptonizing hot clouds are now in progress. In the meantime we neglect such possible effects and use cold cloud results in this discussion.

A common feature to all cloud configurations studied is the development of a minimum in the degree of polarization for a particular observer angle. This angle moves toward the equator for the more relativistic clouds. For

rotating clouds, this is associated with a rotation of the polarization plane. Generally, the polarization features for an equatorial observer resemble the Newtonian results (though there may be changes in the degree of polarization), with relativistic effects becoming prominent as the observer moves toward the pole. The deviation from the Newtonian results takes place nearer to the equator, and over a larger range in θ_0 , for the more relativistic clouds. Note also that a relativistic, rotating spherical cloud can give appreciable polarization for the smaller polar angle observers.

Current estimates of the inclination angle of Cyg X-1 give an observation angle which lies in the polarization-angle transition region, and the minimum of the degree of polarization for a relativistic, geometrically thick cloud. It is possible, therefore, that for high energies the polarization from Cyg X-1 will be small because of this minimum.

For a power-law spectrum emitted by an isothermal and homogeneous cloud there is no energy dependence of the degree or angle of polarization (over the energy range in which the radiation is dominated by the cloud and over which the same power law holds). Lightman and Shapiro (1975) have pointed out that one should be able to observe variations of the polarization features between the low-energy X-rays coming from an external thin disk, and the higher energy X-rays coming from the cloud. Newtonian calculations predict a 90° difference in the polarization angle between the emissions from the two regions. We suggest that only the lowest energy X-ray data should be interpreted according to Chandrasekhar's Newtonian calculation to give the inclination angle of the disk's plane and the angle of observation. A rotation of the polarization with increasing energy followed by constant polarization features at still higher energies would indicate the existence of an inner cloud, and a non- 90° rotation would suggest a general-relativistic effect. The degree of polarization and the amount of rotation relative to the lower-energy X-ray data can be used further as a consistency check for the model (compatibility of the cloud's radius and shape, etc.).

In addition, for a fixed observer energy, one can expect temporal variations of the polarization features of the radiation emitted by an inner cloud. Observers may detect changes in the plane and degree of polarization if the size of the cloud varies, giving rise to a general-relativistically induced time dependence to the polarization properties. Such changes could be associated with spectral and intensity changes. In particular it is important to see if there are any temporal changes in the polarization features of Cyg X-1 which are correlated with the spectral intensity changes between the two states of this source.

Strong magnetic fields ($\geq 10^8$ gauss) in the source lead to Faraday rotation which changes the polarization of the X-radiation. A homogeneous magnetic field leads to both depolarization and rotation of the polarization plane; a chaotic field causes only depolarization. In both cases the influence of the magnetic field is measured (Gnedin and Silant'ev 1977) by the depolarization parameter $120(B/10^8 \text{ gauss})(1 \text{ keV}/E)^2$. Equipartition arguments and more detailed analysis (Eardley and Lightman 1975) lead to a maximum chaotic magnetic field of order 10^8 gauss. This is sufficient to depolarize the X-radiation below 10 keV. However, a chaotic field influences mainly the degree and not the angle of polarization, and its depolarization has a typical E^{-2} dependence. These features enable us to distinguish between strong magnetic and strong general-relativistic effects. Strong magnetic fields do not have to exist in disks. In particular, the measurement of Novick *et al.* (1977) of 3% linear polarization from Cyg X-1 suggests that such a strong depolarization does not take place in this source.

Further refinement of the theoretical model is essential. The most important step is evaluation of the polarization from hot Comptonizing clouds. In addition, development of more accurate disk models which could be used as "physical input" for the polarization calculation is needed. However, even at this stage the importance of more detailed polarization measurements is clear. It is hoped that such a measurement will enable us to solve some of the questions about compact X-ray sources.

It is a pleasure to acknowledge many helpful discussions with J. Miller, R. Novik, R. Penrose, and D. W. Sciama. One of us (T. P.) is indebted to the Department of Astrophysics at Oxford for hospitality during the beginning and completion of this work, and to SRC and to NSF grant PHY77-22489 A01, University of Texas, for financial support. P. A. C. and R. F. S. acknowledge SRC studentships while this research was done.

REFERENCES

- Angel, J. R. P. 1969, *Ap. J.*, **158**, 219.
 Bardeen, J. M., Press, W. H., and Teukolsky, S. A. 1972, *Ap. J.*, **178**, 347.
 Berestetskii, V. B., Lifshitz, E. M. and Pitaevskii, L. P. 1971, *Relativistic Quantum Theory*, Part I (New York: Pergamon Press).
 Boyer, R. H., and Lindquist, R. W. 1967, *J. Math. Phys.*, **8**, 265.
 Carter, B. 1968, *Phys. Rev.*, **174**, 1559.
 Chandrasekhar, S. 1960, *Radiative Transfer* (New York: Dover).
 Connors, P. A., and Stark, R. F. 1977, *Nature*, **269**, 128.
 Cunningham, C. T. 1975, *Ap. J.*, **202**, 788.
 ———. 1976, *Ap. J.*, **208**, 534.
 Cunningham, C. T., and Bardeen, J. M. 1973, *Ap. J.*, **183**, 237.
 De Felice, F. 1968, *Nuovo Cimento B*, **57**, 351.
 Eardley, D. M., and Lightman, A. P. 1975, *Ap. J.*, **200**, 187.
 Eardley, D. M., Lightman, A. P., Shakura, N. I., Shapiro, S. L., and Sunyaev, R. A. 1978, *Comments Ap.*, **7**, 151.
 Gnedin, Yu. N., and Silant'ev, N. A. 1977, *Pis'ma Astr. Zh.*, **3**, 258 (English transl. *Soviet Astr. Letters*, **3**, 136 [1977]).
 Horak, H. G. 1954, *Ap. J.*, **119**, 642.
 Kerr, R. P. 1963, *Phys. Rev. Letters*, **11**, 237.
 Lightman, A. P., and Shapiro, S. L. 1975, *Ap. J. (Letters)*, **198**, 173.
 Misner, C. W., Thorne, K. S., and Wheeler, J. A. 1973, *Gravitation* (San Francisco: Freeman) (MTW).
 Novick, R., Weisskopf, M. C., Silver, E. H., Kestenbaum, H. L. Long, K. S., and Wolff, R. S. 1977, *Ann. NY Acad. Sci.*, **302**, 213.
 Novikov, I. D., and Thorne, K. S. 1973, in *Black Holes*, ed. B. DeWitt and C. DeWitt (New York: Gordon & Breach), p. 345.
 Page, D. N., and Thorne, K. S. 1974, *Ap. J.*, **191**, 499.

- Payne, P. G., and Eardley, D. M. 1977, *Ap. Letters*, **19**, 39.
 Pineault, S. 1977, *M.N.R.A.S.*, **179**, 691.
 Piran, T. 1976, Ph.D. thesis, Hebrew University.
 Piran, T., and Shaham, J. 1977a, *Phys. Rev. D*, **16**, 1615.
 ———. 1977b, *Ap. J.*, **214**, 268.
 Pozdnyabov, L. A., Sobol', I. M., and Sunyaev, R. A. 1976, *Pis'ma Astr. Zh.*, **2**, 140 (English transl. *Soviet Astr. Letters*, **2**, 55 [1976]).
 Pringle, J. E., and Rees, M. J. 1972, *Astr. Ap.*, **21**, 1.
 Rees, M. J. 1975, *M.N.R.A.S.*, **171**, 457.
 Sandford, M. T., and Pauls, T. A. 1973, *Ap. J.*, **179**, 875.
 Shakura, N. I. 1972, *Soviet Astr.—AJ*, **16**, 532.
 Shakura, N. I., and Sunyaev, R. A. 1973, *Astr. Ap.*, **24**, 337.
 Shapiro, S. L. 1973, *Ap. J.*, **180**, 531.
 Shapiro, S. L., Lightman, A. P., and Eardley, D. M. 1976, *Ap. J.*, **204**, 187.
 Stark, R. F., and Connors, P. A. 1977, *Nature*, **266**, 429.
 Thorne, K. S., and Price, R. H. 1975, *Ap. J. (Letters)*, **195**, L101.
 Walker, M., and Penrose, R. 1970, *Commun. Math. Phys.*, **18**, 265.
 Wilkins, D. 1972, *Phys. Rev. D*, **5**, 814.

P. A. CONNORS and R. F. STARK: Department of Astrophysics, South Parks Road, Oxford, OX1 3RQ, England
 TSVI PIRAN: Institute for Advanced Study, Princeton, NJ 08540